The Effects of Geometric and Loading Imperfections on the Response and Lower-Bound Buckling Load of a Compression-Loaded Cylindrical Shell

Benedikt Kriegesmann[*]
Institute of Structural Analysis, Leibniz Universität Hannover, Germany

Mark W. Hilburger[†]
NASA Langley Research Center, Hampton, Virginia, 23681

and

Raimund Rolfes [‡]
Institute of Structural Analysis, Leibniz Universität Hannover, Germany

Results from a numerical study of the buckling response of a thin-walled compression-loaded isotropic circular cylindrical shell with initial geometric and loading imperfections are used to determine a lower bound buckling load estimate suitable for preliminary design. The lower bound prediction techniques presented herein include an imperfection caused by a lateral perturbation load, an imperfection in the shape of a single stress-free dimple (similar to the lateral pertubation imperfection), and a distributed load imperfection that induces a nonuniform load in the shell. The ABAQUS finite element code is used for the analyses. Responses of the cylinders for selected imperfection amplitudes and imperfection types are considered, and the effect of each imperfection is compared to the response of a geometrically perfect cylinder. The results indicate that compression-loaded shells subjected to a lateral perturbation load or a single dimple imperfection, and a nonuniform load imperfection, exhibit similar buckling behavior and lower bound trends and the predicted lower bounds are much less conservative than the corresponding design recommendation NASA SP-8007 for the design of buckling-critical shells. In addition, the lateral perturbation technique and the distributed load imperfection produce response characteristics that are physically meaningful and can be validated via laboratory testing.

Nomenclature

a	=	amplitude of boundary imperfection
BL	=	buckling load
cp	=	circumferential position
F	=	force, applied in axial direction
L	=	cylinder length
P	=	perturbation load, applied perpendicular to cylinder axis
R	=	cylinder raqdius
t	=	cylinder wall thickness
u	=	axial displacement / end shortening
y_t	=	width of boundary imperfection

[*] PhD studend, Institute of Structural Analysis, Appelstr. 9A, 30167 Hannover, Germany.
[†] Senior Research Engineer, NASA Langley Research Center, Hampton, Virginia, 23681.
[‡] Director, Institute of Structural Analysis, Appelstr. 9A, 30167 Hannover, Germany.

I. Introduction

THE design of light-weight, thin-walled, circular cylindrical shells used in aerospace applications, is typically governed by global buckling constraints. For circular cylinders subjected to axial compression, linear buckling analyses predict un-conservative buckling or critical loads when compared to corresponding experimental results. This un-conservative prediction and the corresponding uncertainty in the actual buckling load of the as-built structure can lead to significant challenges for the designer of these structures. The traditional approach for designing a thin-walled, buckling-resistant shell structure is to predict the buckling load of the shell with a deterministic, linear bifurcation buckling analysis, and then to reduce this predicted load with an empirical 'knockdown' factor. The analysis is usually based on nominal structural dimensions and material properties of an idealized, geometrically perfect shell. The empirical knockdown factor is intended to account for the difference between the predicted buckling load and the actual buckling load for the shell determined from tests. For example, the design knockdown factor used in the design of buckling-resistant unstiffened cylindrical shells is often based on the `lower-bound' design recommendations reported in NASA SP-8007.[1] This design philosophy has been used successfully in the design of many launch vehicle structures around the world. However, in recent times new high-fidelity analysis results and experimental results show that this design recommendation can be overly conservative, or can potentially even result in un-conservative designs if the empirical data are not representative of the design of interest.

While it is generally recognized that initial geometric shell-wall imperfections are a major contributor to the difference between the predicted shell buckling loads and the experimentally measured loads, the traditional sources of design knockdown factors do not include data or information related to the sensitivity of the response of a shell to other forms of imperfections. In addition, the traditional sources of design knockdown factors do not include information for structures made from state-of-the-art materials and manufacturing processes. Recent studies have shown that traditional initial geometric shell-wall imperfections, and other nontraditional forms of imperfections or variations in geometric and material parameters, loading conditions, and boundary conditions can significantly affect the buckling load of a compression-loaded composite shell structure (see e.g. Refs. 2–5). These studies have shown that when structural details such as as-measured shell-wall geometry, shell wall thickness, and non-uniform loading are included in a high-fidelity analysis, the buckling load and transient dynamic collapse behavior can be predicted accurately. However, these structural details are typically not known a priori and, thus, designers have had to resort to other methods in order to predict conservative values of the critical load for design. To this end, analysis-based lower bound buckling load predictions have been proposed and two methods will be presented. The first is an approach that uses a lateral perturbation load to create a local dimple-shaped imperfection in the shell wall (see Ref. 3). This dimple is similar to the type of dimple that forms in a compression-loaded shell at the onset of buckling as observed in tests and is thus a physically meaningful initial imperfection or perturbation. In this analysis-based lower-bound approach, the perturbation load is applied before the axial load is applied and is held constant during the application of the axial load. It has been determined that, for unstiffened composite cylinders, there exists a range of lateral perturbation loads where the shell buckling load is very sensitive to changes in the magnitude of this perturbation load. However, above a certain threshold value of the perturbation load, the buckling load appears to reach a minimum value or *lower bound* and is not sensitive to variations in the perturbation load. The buckling load at the threshold value is thought to be a reasonable approximation of a lower bound to the buckling load of the shell. Finally, the effects of non-uniform loading on the nonlinear response and buckling load of a compression-loaded shell is presented. The non-uniform load is assumed to be in the form of a local perturbation in the axial displacement applied to the end of the shell and is intended to simulate the non-uniform loading surface that can occur in a test article or fit-up mismatch at the interface surfaces between launch vehicle components.

In this study, numerically predicted responses of a geometrically perfect and imperfect thin-walled, isotropic circular cylinder subjected to an axial compression load are used to compare several lower bound buckling load prediction methods. The lateral perturbation load imperfection and nonuniform load or load imperfection described above are used for predicting lower bound buckling loads. The response of a geometrically perfect cylinder is also determined to serve as a baseline to which the imperfect cylinders can be compared.

II. Numerical model

An unstiffened isotropic shell is used for the numerical investigations presented herein and is based on a test article that was recently manufactured and tested at NASA Langley Research Center. The shell has a length L = 31 inches and a radius R = 9 inches, corresponding to an L/R = 3.44, and was fabricated by rolling a flat sheet of 0.040-in-thick 2024 aluminum into a cylinder and the two longitudinal free edges are attached together by using a double-overlap riveted splice joint, referred to as a *splice joint*. This splice joint is approximately 2 inches wide and 0.12 in.

thick and is included in the model by adjusting the thickness of the shell wall in the region of this splice (see illustration in Figure 1). The geometry and material properties of the shell are listed in Table 1. Both ends of the shell are assumed to be clamped and the compression load is applied to the shell by imposing a uniform end-shortening displacement to one end of the shell. The nonlinear and buckling analyses were conducted using the ABAQUS finite element code. Four node shell elements with reduced integration were used (S4R elements). A mesh convergence study indicated that a mesh with 110 elements in axial direction and 202 elements in circumferential direction provides sufficient accuracy. Clamped boundary conditions are simulated by connecting the nodes at the end of the shell to a master node via rigid links and the load is then applied to the master node. Geometrically nonlinear quasi-static analyses were conducted under displacement control and linear elastic material behavior was assumed. Simulations with an elastic-plastic material model showed that yielding occurs in the postbuckling range, but the buckling load was not affected by this yielding and is neglected in this study.

Table 1. Characteristics of the metal cylinder

Cylinder geometry	**Splice joint geometry**	**Cylinder and splice joint material properties**
Length: L = 31 in = 787.4 mm	Width: 2 in = 50.8 mm	Young'smodulus: $E = 10.6 \cdot 10^6$psi = 73084.4 N/mm^2
Radius: R = 9 in = 228.6 mm	Thickness: 3 t = 0.12 in = 3.048 mm	Poisson's ratio: $\nu = 0.3$
Thickness: t = 0.04 in = 1.016 mm		Yield stress: σ_Y = 50 ksi = 344.7 N/mm^2
		Yield strain: $\varepsilon_Y = \sigma_Y/E = 4.72 \cdot 10^{-3}$

III. Effects of Initial Imperfections

The effects of several different types of initial imperfections on the nonlinear and buckling response of a thin-walled compression-loaded shell are described in this section. The imperfections considered include a local dimple caused by applying a small-magnitude lateral perturbation load, and a distributed load imperfection that induces a nonuniform load in the shell. In addition, the effects of various combinations of initial imperfections on the buckling response will be presented. Some highlights from the numerical study are presented in the following subsections.

A. Single lateral perturbation load

The effect of a lateral perturbation load on the buckling response of a compression-loaded shell is presented. The axial location is held constant at the shell mid-length. The circumferential location of the lateral perturbation load is denoted by cp and can vary from 0.0 to 2πR, where 0.0 corresponds to the location of the splice joint. A sketch of the compression-loaded shell with a lateral perturbation load is shown in Figure 1.

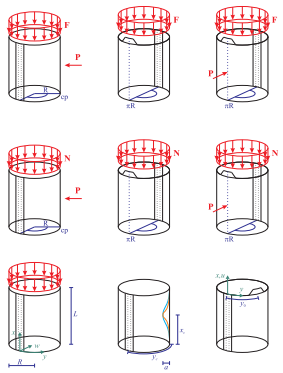

Figure 1: Sketch of axially compressed shell with lateral perturbation

Typical load (F) versus end-shortening (u) curves for a compression-loaded cylinder with a lateral perturbation load imperfection are shown in Figure 2.

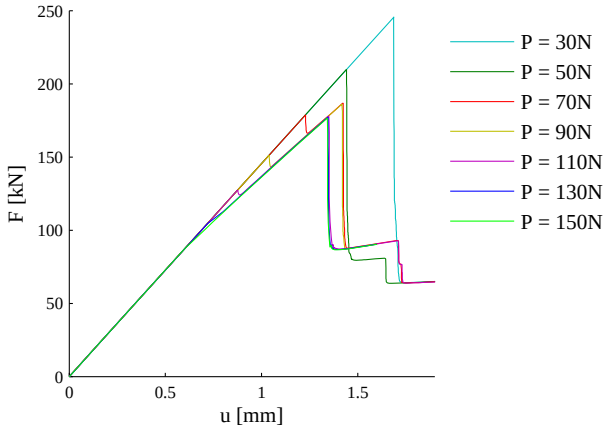

Figure 2: Axial load versus end-shortening curves with cp = πR

The load versus end-shortening results indicate that the shell exhibits a linear pre-buckling response up to the first buckling point and there is no noticeable change in effective prebuckling axial stiffness for different values of the perturbation load. For relatively small-magnitude perturbation loads, e.g., loads equal to 30N and 50N, the first buckling point corresponds to the overall global collapse of the shell. In contrast, for larger magnitude perturbation loads, the first buckling point corresponds to a stable local buckling event in which an ellipse-shaped inward buckle forms in the shell wall. The shell exhibits a slight reduction in axial stiffness as indicated by the slope of load-end-shortening response curves and can then sustain additional axial load until global collapse occurs.

Typical shell wall displacements during the response of a compression-loaded shell with a lateral perturbation load P = 110N located diametrically opposite of the splice joint (cp = πR)are shown in Figure 3 (note: the positive displacements in the contour plots correspond to inward radial deformation of the shell wall).The load level that corresponds to a given displacement contour is marked on the load-shortening curve with a red open circle. For small magnitude perturbation loads, a small ellipse-shaped dimple appears in the pre-buckling region similar to that shown in Figure 3a. The size and magnitude of the dimple does not grow significantly until global buckling is initiated. In contrast, for sufficiently large magnitude perturbation loads, the small dimple caused by the lateral perturbation load grows in magnitude abruptly as the first point of local instability is passed. This first buckling point corresponds to a local buckling event and causes a drop in axial load (Figure 3b). The buckle then grows in magnitude until global buckling occurs (Figure 3c).

Shell buckling load (BL) versus lateral perturbation load (P) curves for three different circumferential positions of the perturbation load are shown in Figure 4. The open circles connected by solid lines correspond to global buckling loads and the open circles connected by dashed lines correspond to local buckling loads for cases with cp equal to πR/2 and πR, in which a local buckling response precedes the global buckling. The results indicate that the global buckling load is sensitive to variations in the lateral perturbation load if the perturbation load is between 0.0 and 70N as shown by the significant reduction in buckling load as the perturbation load is increased. However, if the perturbation load exceeds 70N, then the global buckling load is no longer sensitive to variations in the magnitude of the perturbation load and a *lower bound* of approximately 176N is obtained. The results also indicate that, as long as the perturbation load is not located on the splice joint, the circumferential location of the perturbation does not appear to influence the buckling behavior significantly. Finally, it is observed that the buckling load of the shell is only slightly affected by the lateral perturbation loads considered herein when applied to the splice joint.

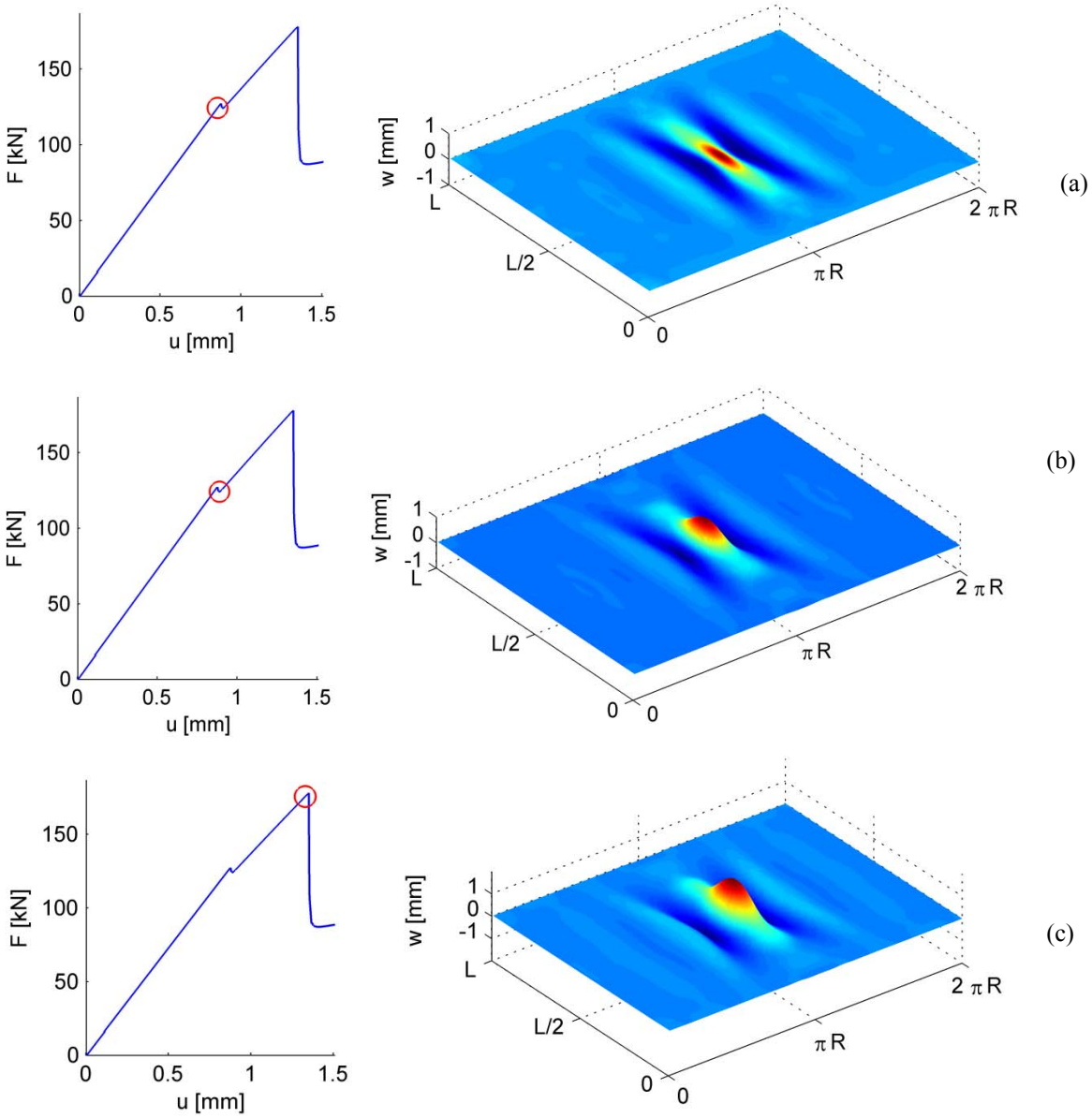

Figure 3: Displacement response of a shell with single perturbation load, P = 110N at cp = 0.5 $2\pi R$

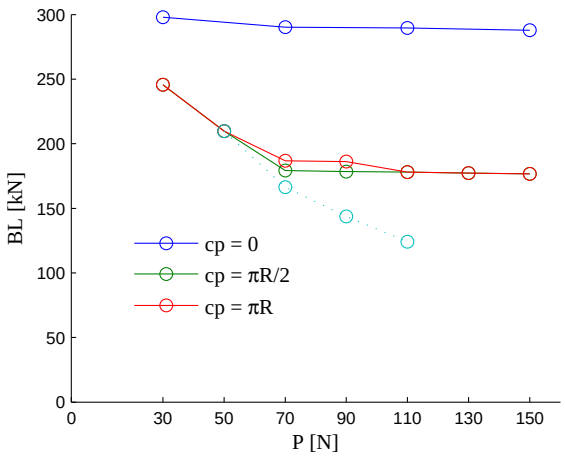

Figure 4: Buckling load versus lateral perturbation load

B. Distributed loading imperfection

In this section, the influence of an axial loading or boundary imperfection is presented. Such a boundary imperfection can come about in an as-built structure due to manufacturing tolerances or irregularities and can cause nonunifom loading in the structure when joined to adjacent structure. Geier et al.[6] used a shim layer to apply such a boundary imperfection in experimental tests on composite shells. Hühne et al.[7] showed that also for this type of imperfection a lower bound of buckling load can be found. In the present study, these findings shall be put into context with the influence of a lateral perturbation load, discussed in the previous section. Therefore, a loading imperfection is simulated in the shell by including an axial perturbation or imperfection in the geometry of one of the loaded edges of the shell as shown in Figure 5. This geometric imperfection in the axial direction is defined by its location y_0, width y_t, amplitude a and the length y_d of the transition region (see Figure 6). For the study considered herein, the loading imperfection is located diametrically opposite to the slice joint corresponding to $y^* = \pi R$.

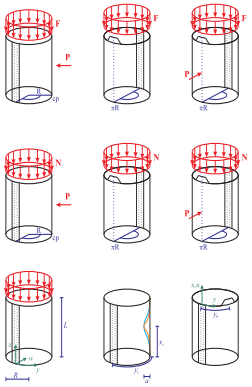

Figure 5: Sketch of cylinder with an imperfection on the loaded edge

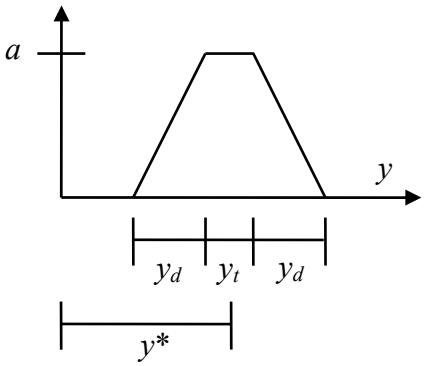

Figure 6: Shape function of shim layer boundary imperfection

Results from the corresponding geometrically perfect shell indicated that the circumferential wavelength of the displacement pattern at the onset of buckling is about 55mm and the circumferential wavelength of post buckling pattern is approximately 205mm.Based on the characteristic dimensions of the pre-buckling and post-buckling displacements, load imperfection widths between 20mm and 100mm were studied with the assumption that this range of widths would be the most detrimental to the buckling load of the shell. Similarly, the amplitude of the

loading imperfection was chosen to be between 0 and 20% of the critical end-shortening value for the geometrically perfect shell.

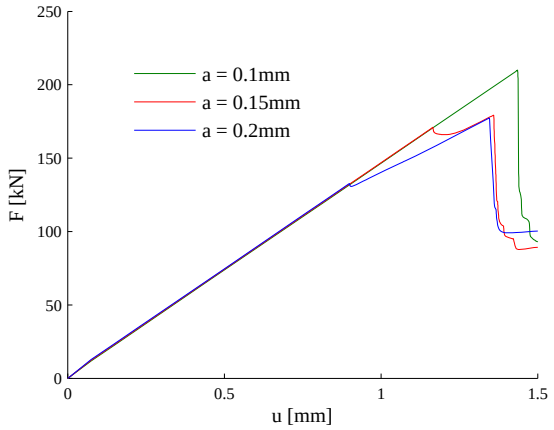

Figure 7: Load versus end shortening for three different loading imperfection amplitudes.

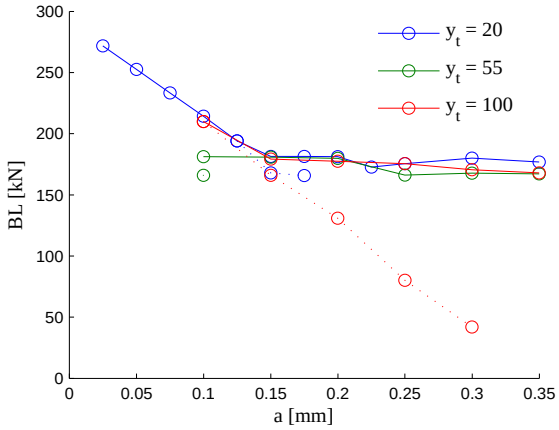

Figure 8: Buckling load versus loading imperfection amplitude.

Typical load versus end-shortening curves for a shell with three different load imperfection amplitudes, a = 0.1mm, 0.15mm, and 0.2mm, and a y_t of 55mm are shown in Figure 7. Buckling load BL versus imperfection amplitude for three different values of imperfection width y_t are shown in figure 8.Buckling loads are indicted in Figure 8 by open circle symbols. Global buckling loads are connected by solid lines and local buckling loads are connected by dashed lines. The results indicate that a shell with this type of loading imperfection exhibits similar behavior to the corresponding shell with a lateral perturbation load presented in the previous section. More specifically, as the amplitude of the loading imperfection increases from 0.025mm to 0.15mm, the global buckling load decreases significantly. However, an additional increase in the amplitude of the imperfection beyond 0.15mm has only a slight effect on the global buckling load and the shell obtains a lower bound buckling load value of approximately 170kN (see Figure 8), 3% less than the lower bound predicted for the shell with a lateral perturbation load. In addition, the results indicate that the reduction in global buckling load is, for the most part, insensitive to the width of the loading imperfection considered.

Typical shell wall displacements during the response of a compression-loaded shell with a 100mm wide loading imperfection with an amplitude of 0.2mm are shown in Figure 9 (note: the positive displacements in the contour plots correspond to inward radial deformation of the shell wall). The load level that corresponds to a given displacement contour is marked on the load-shortening curve with a red open circle. During initial loading of the shell a local ellipse-shaped dimple forms in the shell wall near the imperfect boundary (see Figure 9a). This dimple causes a local buckling event to occur near the boundary and is associated with a slight drop in axial load (see Figure 9b).Upon further loading, this local buckle moves towards the mid-length of the shell until global buckling occurs (see Figure 9c).

Thus, it is significant to note that while the loading imperfection is physically very different from the lateral perturbation and single dimple imperfection, they both cause the compression-loaded shell to exhibit similar nonlinear response and buckling characteristics. Furthermore this may enable the development of a unified theory of imperfection sensitivity that can be used as the basis for new design criteria for buckling-critical shells.

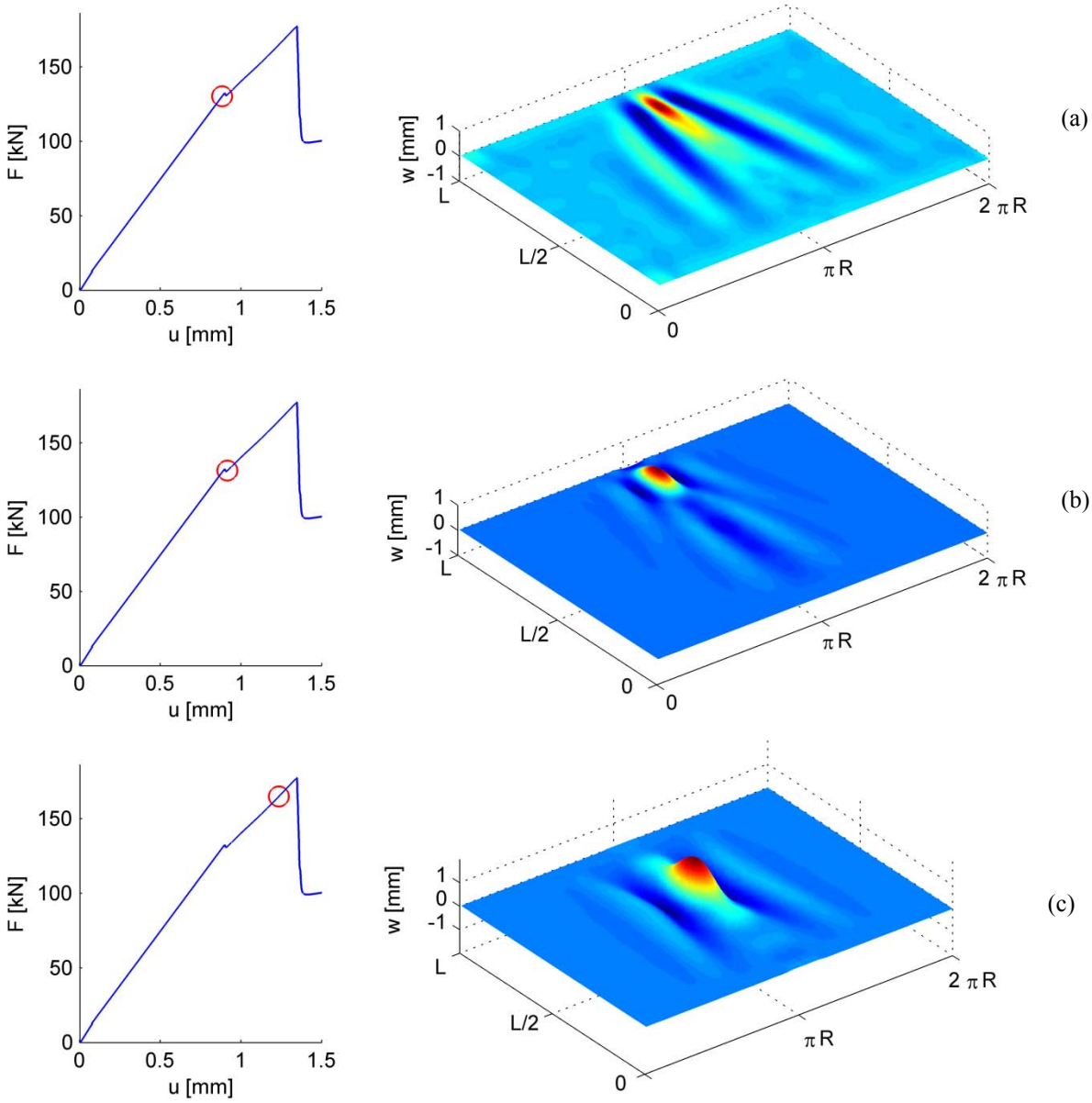

Figure 9: Displacement pattern of shell with shim layer boundary imperfection, a = 0.2mm, y_t = 100mm

C. Combined lateral perturbation load and loading imperfection

In this section the effect of combining a single perturbation load with a distributed loading imperfection is presented. Perturbation load and the loading imperfection are located diametrically opposite the splice joint as shown in Figure 10. The axial position of the perturbation load is located at the mid length of the shell. The width of the loading imperfection is held fixed at 80mm and the amplitudes of the lateral perturbation and loading imperfection are varied independently.

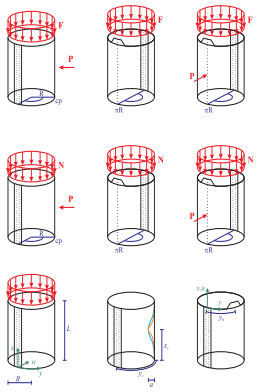

Figure 10: Lateral perturbation load and concentrated boundary imperfction

Typical buckling-load versus perturbation-load and buckling-load versus load-imperfection-amplitude curves are shown in Figure 11 and Figure 12, respectively. The open circles connected by solid lines correspond to global buckling loads and the open circles connected by dashed lines correspond to local buckling loads for cases in which a local buckling response precedes global buckling. In general, these buckling-load trends are similar to the previous results presented for a compression loaded cylinder subjected to a lateral perturbation load (Figure 4) or load imperfection (Figure 8). In addition, the results show that the buckling load lower bound is equal to 170kN and is about 3.4% lower than the corresponding lower bound obtained by applying only a single perturbation load or loading imperfection.

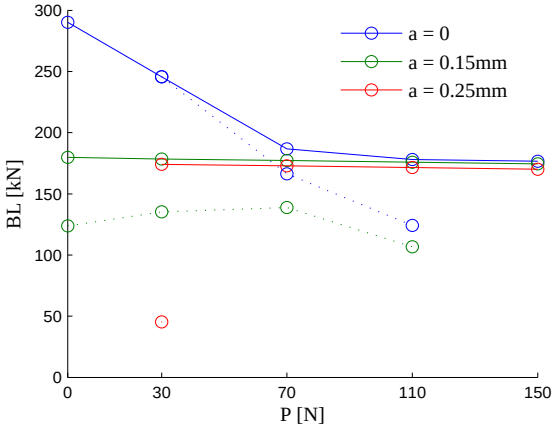

Figure 11: Buckling load versus perturbation load for different boundary imperfection amplitudes

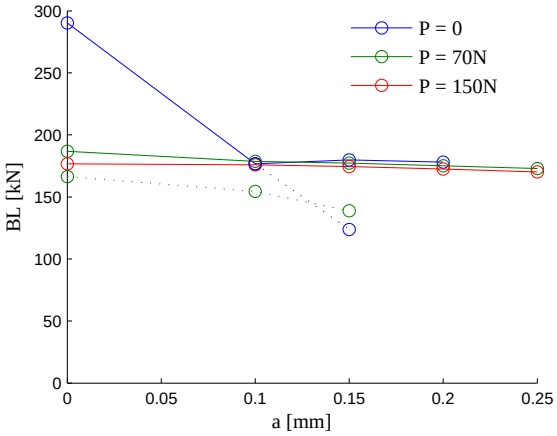

Figure 12: Buckling load versus boundary imperfection amplitude for different perturbation loads

IV. Summary

The results presented suggest that, regardless of the type of imperfection, whether alone or in combination, the lower bound buckling load for the compression-loaded shell considered herein is approximately 170kN. Furthermore, it appears that the primary mechanism associated with the buckling response is the formation of a single buckle and that this singe buckle can form directly, in the case of the lateral perturbation load, or indirectly, as in the case of the applied loading imperfection.

What is more compelling is the fact that, while the loading imperfection is physically different from the lateral perturbation imperfection and single dimple imperfection, they both cause the compression-loaded shell to exhibit similar nonlinear response and buckling characteristics. It is hoped that this may enable the development of a simple unified theory of imperfection sensitivity that can be used as the basis for new design criteria for buckling-critical shells.

Acknowledgments

This work was conducted during the first authors research stay at NASA Langley Research Center and was a part of the NASA Engineering and Safety Center (NESC) Shell Buckling Knockdown Factor Project, NESC Assessment #:07-010-E.

References

[1]*Buckling of Thin-Walled Circular Cylinders*, NASA SP-8007, 1968.

[2]Hilburger, M. W. & Starnes Jr, J. H., "Effects of Imperfections on the Buckling Response of Compression-Loaded Composite Shells," *International Journal of Non-Linear Mechanics*, Vol. 37, pp. 623–643, 2002.

[3]Hühne, C., Rolfes, R., Breitbach, E. & Teßmer, J., "Robust Design of Composite Cylindrical Shells Under Axial Compression – Simulation and Validation," *Thin-Walled Structures*, Vol. 46, 2008, pp. 947–962.

[4]Degenhardt, R. *et al.*, "Investigations on Imperfection Sensitivity and Deduction of Improved Knock-down Factors for Unstiffened CFRP Cylindrical Shells," *Composite Structures* Vol. 92, 2010, pp. 1939–1946.

[5]Kriegesmann, B., Rolfes, R., Hühne, C. & Kling, A.. "Fast Probabilistic Design Procedure for Axially Compressed Composite Cylinders," *Composites Structures*, Vol. 93, 2011, pp. 3140–3149.

[6]Geier, B., Klein, H. & Zimmermann, R., "Experiments on Buckling of CFRP Cylindrical Shells Under Non-Uniform Axial Load," presented at the International Conference on Composites Engineering, New Orleans, Lousiana, 1994, pp. 28–31.

[7]Hühne, C., Zimmermann, R., Rolfes, R. & Geier, B., "Sensitivities to Geometrical and Loading Imperfections on Buckling of Composite Cylindrical Shells," presented at the European conference on spacecraft structures, materials and mechanical testing, Toulouse, France, 2002.